Yoo JH, Kockert H, Mullaney JC, Stephens SL, Evans CJ, Walker NR, LeRoy RJ.

Vibrational Energies and Full Analytic Potential Energy Functions ofPbI and InI from Pure Microwave Data.

***Journal of Molecular Spectroscopy* 2016**

DOI: http://dx.doi.org/10.1016/j.jms.2016.08.012

Vibrational Energies and Full Analytic Potential Energy Functions of PbI and InI from Pure Microwave Data

J. H. Yoo[a], Hansjochen Köckert[b], J. C. Mullaney[b], S. L. Stephens[b,c], C. J. Evans[d], Nicholas R. Walker[b], Robert. J. Le Roy[a]

[a]*Department of Chemistry, University of Waterloo, Waterloo, Ontario N2L 3G1, Canada*
[b]*School of Chemistry, Bedson Building, Newcastle University, Newcastle upon Tyne, Tyne and Wear, NE1 7RU, U.K.*
[c]*Current address: Chemistry Department, 360 Parker Building, University of Manitoba, Winnipeg, MB, R3T 2N2, Canada*
[d]*Department of Chemistry, University of Leicester, Leicester LE1 7RH, United Kingdom*

Abstract

Pure rotational spectra of PbI and InI are interpreted to yield a full analytic potential energy function for each molecule. Rotational spectra for PbI have been retrieved from literature sources to perform the analysis. Rotational transition frequencies for excited vibrational states of InI ($0 < v < 11$) are measured during this work. Ignoring hyperfine splittings, B_v and D_v values are used to generate a set of "synthetic" pure $R(0)$ transitions for each vibrational level. These are then fitted to an "Expanded Morse Oscillator" (EMO) potential using the direct-potential-fit program, **DPOTFIT**. The well-depth parameter, $\mathfrak{D}_e$, is fixed at a literature value, while values of the equilibrium distance r_e and EMO exponent-coefficient expansion (potential-shape) parameters are determined from the fits. Comparison with potential functions determined after including older mid-IR and visible electronic transition data shows that our analysis of the pure microwave data alone yields potential energy functions that accurately predict (to better than 1%) the overtone vibrational energies far beyond the range spanned by the levels for which the microwave data is available.

Keywords:

Rotational spectroscopy, potential energy fitting, lead iodide, indium iodide

Email addresses: nick.walker@newcastle.ac.uk (Nicholas R. Walker), rleroy@scienide2.uwaterloo.ca (Robert. J. Le Roy)

1. Introduction

Opportunities and advantages presented by broadband rotational spectroscopy are extensively described in a number of publications [1, 2]. Amongst these are the opportunity to measure spectra spanning bandwidths exceeding 10 GHz in a single experiment of short duration; and the possibility that spectral patterns can be more easily identified and compared. Many transitions are observed simultaneously and transition intensities reflect intrinsic molecular properties rather than a frequency-dependent instrument design parameter. Each of these advantages is useful in the context that rotational transition frequencies can be simultaneously recorded and compared for many different vibrational states. The 'conventional' approach to analyzing such data is to fit those for each vibrational level separately using a program such as Western's **PGOPHER** [3] to determine distinct values of rotational and magnetic splitting parameters for each level. This was the first step in the present study. However, other than providing a good estimate of the equilibrium bond length, this provides little insight into the vibrational properties or the potential energy function which governs the molecule's dynamical behaviour. The present work expands on this approach by using the information about the molecule's dynamical behaviour contained in the rotational constants B_v and D_v , and their v-dependence, to determine full analytic potential functions for both PbI and InI.

The microwave spectrum of PbI was recorded recently in our laboratories and presented together with derived geometrical parameters of the molecule in 2014 [4]. In the present work, the extensive results presented in [5] are combined with results obtained by other workers for different wavelength ranges [6–11] and used for the potential energy function fitting described in Section 3.2.2. The microwave spectrum of InI has been explored by several previous works [12, 13] with the most recent study having been performed in 2006 [14]. Rotational transition frequencies are measured and parameters in a model Hamiltonian determined for vibrational levels from $v = 4$ to 11 for the first time herein. The present work then combines our new MW results with older electronic transition data for InI in the visible region [15–18] to determine a simple potential energy function (PEF) which provides the most compact, accurate description of the mechanical behaviour of this molecule. It differs from previous studies in that it shows for the first time that it is feasible to determine analytic potential energy functions for PbI and InI from pure rotational data that provide realistic predictions of the vibrational level spacings over an extended domain. In particular, the direct-potential-fits (DPFs) to the microwave data alone are followed by fits to a combination of the microwave data with all available electronic data for these two species to obtain full analytic PEFs that accurately represent all available data for the ground electronic states of PbI and InI. Comparisons between

the results of the two fits indeed demonstrate that in the absence of any infrared or electronic data, DPF fits to v-dependent microwave data can yield predictions of vibrational level energies that are remarkably accurate on a domain far broader than its v-range.

2. Experimental Methods

The broadband microwave spectrum of InI was measured using a chirped-pulse Fourier-transform microwave (CP-FTMW) spectrometer fitted with a laser ablation source. Detailed descriptions of the spectrometer and laser ablation source were previously provided in [1] and [19]. A gas sample containing about 1.5% CF_3I is diluted in argon and prepared at a total pressure of 6 bar. The sample is pulsed into the vacuum chamber of the spectrometer and passes over the surface of a metal rod that is ablated by a Nd:YAG laser pulse (λ = 532 nm, pulse duration of 10 ns, pulse energy of 20 mJ) before undergoing supersonic expansion. A repetition rate of approximately 1.05 Hz is employed. The rod is continually translated and rotated in order to expose a fresh surface to each laser pulse.

The sequence employed to record broadband microwave spectra involves: (i) polarization of the sample by a microwave chirp that sweeps from 6.5 to 18.5 GHz within 1 μs, and (ii) recording of the free induction decay of the molecular emission over a subsequent period of 20 μs. The sequence of (i) and (ii) is repeated eight times within the (about 200 μs) period of the gas nozzle pulse which introduces sample gas into the spectrometer. The free induction decay (FID) of the polarization is digitized using a 25 Gs/s digital oscilloscope after down-mixing against a 19 GHz local oscillator. The time-domain data are averaged to improve the S/N of recorded spectra. Individual transitions are observed with full width at half maximum (FWHM) of 150 kHz after time-domain data are Fourier transformed using a Kaiser-Bessel digital filter. 44k FIDs were averaged in order to record the spectrum of Figure 1.

3. Results

3.1. Assignment of the Rotational Spectra of Vibrational Excited States of InI

Components of the prepared gas sample were probed while undergoing supersonic expansion to reveal rotational transitions of CF_3I and IF in addition to those of InI. Assignments of rotational transitions in the v = 0, 1, 2 and 3 states of the latter were readily achieved through reference to previous studies [12, 13]. A section of the spectrum displaying rotational transitions of InI for a series of vibrational states is displayed in Figure 1. The relative intensities of the rotational spectra of the excited vibrational states correlate with the ratio of the vibrational state populations. However,

the vibrational temperature implied by this ratio does not necessarily provide a good indication of all energy partitioning between vibrational, rotational and translational modes. The events that follow the pulsed laser vaporization of the rod target proceed under conditions that do not allow components of the gas sample to equilibrate. The conditions employed are apparently particularly favourable to the generation of excited vibrational states of PbI and InI. Excited vibrational states are commonly observed in spectra recorded for molecules generated through a combination of laser vaporization and supersonic expansion [20–23].

The most recent study of InI by microwave spectroscopy used a Balle-Flygare FTMW spectrometer [14] to yield accurate transition frequencies for the $v = 0$ state. The results of that earlier work provided a guide to the rotational transition frequencies and hyperfine splitting patterns that could be expected of the rotational spectra of excited vibrational states. For the spectra observed during this work, Western's program **PGOPHER** [3] was used to fit parameters in a model Hamiltonian to the rotational transition frequencies. The Hamiltonian employed is of the form,

$$\boldsymbol{H} \;=\; \boldsymbol{H}_{\rm R} \;-\; \tfrac{1}{6} \sum_{X={\rm In,I}} \mathbf{Q_X} : \mathbf{V_X} \;+\; \sum_{\mathbf{X}={\rm In,I}} \boldsymbol{I_X} \cdot \mathsf{C}^{\mathbf{X}} \cdot \boldsymbol{J} \quad , \tag{1}$$

in which $\boldsymbol{H}_{\rm R}$ is the Hamiltonian for a semi-rigid diatomic rotor. The second term describes the coupling of the nuclear electric quadrupole moment, $\mathbf{Q}_X$, with the electric field gradient $\mathbf{V}_X$ at nucleus X. The third term, $\sum_{X={\rm In,I}} \boldsymbol{I}_X \cdot \mathsf{C}^X \cdot \boldsymbol{J}$, describes the magnetic coupling interactions between each of the nuclear spins, $\boldsymbol{I}_X$, and the rotational angular momentum, $\boldsymbol{J}$. The coupling scheme $\boldsymbol{J} + \boldsymbol{I}_{\rm I} = \boldsymbol{F}_1$; $\boldsymbol{F}_1 + \boldsymbol{I}_{\rm In} = \boldsymbol{F}$ was used. Fitting parameters to measured transition frequencies in the model Hamiltonian yielded the inertial rotational constant B_v, the leading centrifugal distortion constant, D_v, and the nuclear quadrupole coupling constants of the indium and iodine nuclei respectively, $\chi^{\rm In}$ and $\chi^{\rm I}$ for each vibrational level. An earlier study of the rotational spectrum of the ground vibrational level had yielded values of nuclear spin-nuclear spin coupling terms for that level [14]. At the resolution of the present experiment, which is lower than that achieved by the Balle-Flygare FTMW spectrometer employed in 2006, any contribution from nuclear spin-nuclear spin coupling will be insignificant compared with the statistical uncertainties of evaluated parameters. The results of the fit of model parameters to measured transition frequencies obtained during the present work are shown in Table 1, together with details of the number of lines included for each vibrational state. The rotational spectra of vibrational states with $v > 11$ are not sufficiently intense to be included in the fits. Measured transition frequencies and complete details of the fits to determine the spectroscopic parameters shown in Table 1 for each of the vibrational states, $v = 0 - 11$ are provided in the Supplementary Data.

3.2. Potential Energy Function Fitting

3.2.1. Methodology

In a "direct-potential-fit" analysis one starts from a parameterized analytic model potential energy function(s) for the state(s) of interest, solves the radial Schrödinger equation for the upper and lower level of every transition in the data field, and uses non-linear least-squares fits to the experimental data to optimize the model PEF(s). As nuclear spin splitting effects do not carry direct information about the potential energy functions, this type of analysis focuses attention on the "mechanical" information in the spectra, which in this case is the information contained in the rotational constants B_v and D_v obtained from the **PGOPHER** analysis, as presented in Table 1. However, our DPF analysis program [24] can only fit to transition energy data, and not to rotational constants, so the fitted values of these constants and their uncertainties $u(B_v)$ and $u(D_v)$ and their inter-parameter correlation coefficients $\mathbf{C}_{B_v,D_v}$, were used to construct a set of synthetic $R(0)$ transition energies, with appropriate uncertainties, as input to our DPF analysis. In particular, they were generated from the equations:

$$\nu_v^R(J) \;=\; 2\,B_v(J+1) - 4\,D_v(J+1)^3 \tag{2}$$

$$\begin{aligned} u_v(J) \;\equiv\; u\left\{\nu_v(J)\right\} \;=\; \Bigg\{ & \left[\frac{\partial\,\nu_v^R(J)}{\partial\,B_v}\;u(B_v)\right]^2 \;+\; \left[\frac{\partial\,\nu_v^R(J)}{\partial\,D_v}\;u(D_v)\right]^2 \\ & +\;2\;\frac{\partial\,\nu_v^R(J)}{\partial\,B_v}\;u(B_v)\;\frac{\partial\,\nu_v^R(J)}{\partial\,D_v}\;u(D_v)\;\mathbf{C}_{B_v,D_v}\Bigg\}^{1/2} \end{aligned} \tag{3}$$

The values of B_v, D_v and $\mathbf{C}_{B_v,D_v}$ for PbI are taken from Evans *et al.* [5], and those for InI were measured during this work, as described in Section 3.1.

Using the synthetic data sets described above, DPF analyses were performed to determine an optimal model PEF for each species that will represent our synthetic experimental data as accurately as possible. In both cases the PEF model used was an "expanded Morse oscillator" (EMO) function, which has the form of a simple Morse potential in which the exponent coefficient can vary with distance [24–28]:

$$V(r) \;=\; \mathfrak{D}_e\left[1 \;-\; e^{-\beta(r)\cdot(r-r_e)}\right]^2 \tag{4}$$

in which $\mathfrak{D}_e$ is the well depth, r_e the equilibrium internuclear distance, and the exponent coefficient function $\beta(r)$ is written as a simple power series

$$\beta(r) \;=\; \sum_{i=0}^{N_\beta}\;\beta_i\;y_q(r)^i \tag{5}$$

in the dimensionless variable

$$y_q(r) \;=\; \frac{r^q - {r_e}^q}{r^q + {r_e}^q} \tag{6}$$

that maps the infinite domain $r \in [0, \infty)$ onto the finite interval $y_q \in [-1, +1]$.

Since the experimental data for the two systems span only small portions of their potential energy wells, we cannot expect to determine values of $\mathfrak{D}_e$ from our analysis, so these were held fixed at values from the literature. The parameters to be determined from the fits are therefore the equilibrium distance r_e and the EMO exponent-coefficient expansion "potential shape" parameters β_i.

3.2.2. Results for PbI

Although vibrational level spacing data for PbI has been available for a number of years [6], we chose to initiate the present study by considering only the v-dependent pure rotational data. PbI is an open-shell molecule and the PEF analysis was performed for the $^2\Pi_{1/2}$ state. The "synthetic" transition frequencies (calculated as described above) employed were those that correspond with $R(J)$ transitions observed experimentally in the microwave spectra. The synthetic microwave data thus consist $R(J)$ transitions for $J = 4 - 10$ for vibrational levels $v = 0 - 3$, $J = 5 - 10$ for $v = 4$, and $J = 5 - 10$ for $v = 5$ of ^{208}PbI, $R(J)$ transitions for $J = 4 - 9$ for $v = 0 - 2$ of ^{206}PbI and $v = 0$ of ^{207}PbI, and $R(J)$ transitions for $J = 6 - 9$ for $v = 1$ of ^{207}PbI, yielding a total of 68 transition energies with uncertainties ranging from $10^{-7} - 10^{-8}$ cm^{-1}. A classical interpretation of the value of $B_{v=0}$ and of the v-dependence gives us a realistic initial estimate for r_e, but since this initial analysis ignored the earlier (electronic-transition) near-IR work, the data used contained no direct information about the vibrational spacings which could have helped us generate realistic initial estimates of one or two of the leading β_i parameters. Our analysis therefore started with a manual search for an optimal estimate of the leading exponent expansion parameter β_0.

The *Bottom Panel* of Fig. 2 shows how the quality-of-fit dimensionless root-mean-square deviation parameter $\overline{dd}$ varies with trial values of β_0 in fits with r_e and varying numbers of additional β_i parameters as free fitting parameters. From the very first series of fits in which r_e was the only free parameter (green square point and steep curve in the middle of the figure), it is immediately clear where the optimal value of β_0 lies, and the analogous blue and red points and curves showing the results of fits having one or two additional free β_i parameters, respectively, clearly have their minima in the same region. Fits which also had β_3 free were unstable, because of excessive inter-parameter correlation. The *Middle Panel* of Fig. 2 shows how the fundamental vibrational level spacing of these fitted potentials varies as the fixed β_0 value is varied across this domain. It is interesting to see that the results for the three different models (with zero, one, or two free β_i's) are

indistinguishable on this scale. The horizontal dotted line on this panel is the fundamental vibrational band energy predicted by the parameters obtained by Ziebarth *et al.* from their analysis of a number of near infrared electronic transition bands [6]. On the scale of this figure, it is clearly in excellent agreement with the value(s) obtained from our fitted potentials. Finally, as a consistency check, the *Top Panel* of Fig. 2 shows how the centrifugal distortion constants $D_{v=0}$ calculated from our fitted potentials vary with the fixed value of β_0, and compares them to the empirical value of this constant used to generate the synthetic data.

While it is gratifying to see that the pure rotational component of our data set can indeed provide sound information about the well-width vs. energy behaviour which defines vibrational level spacings, on the scale of Fig. 2, the actual discrepancy is actually $\sim$0.5 cm^{-1}, which is an order of magnitude larger than the experimental uncertainty [6], so the microwave data alone do not fully summarize all that is known about the PEF of ground-state PbI. Fortunately, although the detailed linelist [6] obtained by Ziebarth *et al.* and used in their analysis was not reported or archived, the 11 band origins they reported still provide direct measurements of the vibrational spacings for $v'' = 0-3$, with only one 'orphaned' band (4,3) having an upper state that is connected to only a single ground-state level. Including these 10 additional data in our analysis, with assigned uncertainties of 0.05 cm^{-1}, had no significant effect on the quality of fit to the MW data and provides us with a PEF that should be reliable to beyond $v = 5$, which lies almost 900 cm^{-1} above the potential minimum. The middle column of Table 2 presents the parameters defining the PEF obtained from this combination of MW data for $v'' = 0-5$ with the $X2-X1$ band heads spanning the range $v'' = 0-3$, and compares them to the parameters defining the potential based on only the MW data. Within their uncertainties the two sets of parameters are essentially identical.

In an effort to obtain the most comprehensive possible empirical determination of the PEF of ground-state PbI, we introduce a third type of experimental data into this analysis. The first spectroscopic observations of PbI in the 1930's [7–9] were unresolved band heads observed in UV absorption spectroscopy. Wieland and Newburgh [10] extended and reorganized the data in 1952, while Rodriguez *et al.* [11] extended it further and provided some new assignments in 1996. The data reported by Rodriguez *et al.* consist of 128 band heads involving emission into ground state vibrational levels $v'' = 0-40$. While their uncertainties (of $\pm$4 cm^{-1}) are two orders of magnitude larger than those of the near-IR band heads [6] of Ziebarth *et al.*, and seven orders of magnitude larger than those of our MW data, they provide our only direct information about vibrational levels above $v = 5$. Moreover, proper weighting of the various data types means that they effectively contribute to the analysis virtually independent of one another. These 128 band heads were introduced into our analysis in the form of 27 fluorescence series, one associated with each observed

vibrational level of the $A\,^2\Sigma^+_{1/2}$ upper state. Fully accounting for these data in the analysis required the introduction of two additional β_i 'shape' parameters into our model for the PEF of ground-state PbI, cost us a little precision in the representation of the microwave data, and yielded the set of PEF parameters presented in the third column of Table 2.

To summarize our comparison of the three stages of our DPF analysis, the *Lower Panel* of Fig. 3 plots the errors, relative to values generated from our final recomended PEF for PbI (column 3 in Table 2), of overtone energies generated from the MW data alone (blue triangular points, curve, and error bars), and of overtone energies generated from the combination of our MW data with the Ziebarth *et al.* [6] vibrational data for $v = 0 - 3$ (red square points, curve, and error bars). The *Upper Panel* of Fig. 3 then plots those same discrepancies as a percentage of the associated overtone energy. It is interesting to see that across the whole 6000 cm^{-1} overtone range from $v = 1 - 40$, these discrepancies are always smaller than 1% of the associated vibrational energy.

As a last point, we note that the results described above were obtained using only the 39 MW data for the ^{208}Pb^{127}I isotopologue, either alone or in combination with the IR and UV electronic data. However, when the 18 MW data for ^{206}Pb^{127}I and 11 MW data for ^{207}Pb^{127}I were included, the final parameters were essentially unchanged, but for the cases of the first two columns in Table 2, obtaining an optimal fit to the MW data required the introduction of a Born-Oppenheimer breakdown potential-energy (adiabatic) correction term. As usual [24], this BOB correction for a molecule A–B is written as an isotopologue-dependent additive correction to the potential energy function with the form

$$\Delta V^{(\alpha)}_{\rm ad}(r) \;\; = \;\; \frac{\Delta M^{(\alpha)}_{\rm A}}{M^{(\alpha)}_{\rm A}}\, \widetilde{S}^{\rm A}_{\rm ad}(r) \;+\; \frac{\Delta M^{(\alpha)}_{\rm B}}{M^{(\alpha)}_{\rm B}}\, \widetilde{S}^{\rm B}_{\rm ad}(r) \quad , \tag{7}$$

in which $M^{(\alpha)}_{\rm B}$ and $M^{(\alpha)}_{\rm B}$ are the atomic masses of the two atoms forming isotopopogue–α and $\Delta M^{(\alpha)}_{\rm A}$ and $\Delta M^{(\alpha)}_{\rm B}$ are their differences from the analogous atomic masses in the chosen 'reference isotopologue' (here ^{208}Pb^{127}I). Since our MW data involves only a single isotope of atomic iodine, we only have a Pb-atom correction, for which the standard one-term radial strength function expression [23, 24] is

$$\widetilde{S}^{\rm Pb}_{\rm ad}(r) \;\; = \;\; [1 - y_p(r)]\, u^{\rm Pb}_1\, y_p(r) \tag{8}$$

in which $y_q(r)$ is the dimensionless radial variable of Eq. (6) and in this case, $p = q$. From the results in the seventh row of Table 2 we see that within the uncertainties, the values of the fitted BOB parameter $u^{\rm Pb}_1$ in the first two columns were the same. Although the uncertainties are fairly large, we note that including this parameter in the combined-isotopologue analysis of column 1 led to a decrease in the dimensionless standard deviation of by over 30%, so we believe that this isotopic

correction term is physically significant. However, the results in the last column of Table 3 show that the stress imposed on the model by the requirements of a simultaneous fit to vibrational data for levels up to $v = 40$ led to a decrease in the quality of fit to the microwave data, so it should be no surprise that the resulting fitted value of $u_1^{\rm Pb}$ had an uncertainty of over 200%. As a result, in our final fit for this case, this parameter was held fixed at the (common!) value determined from the more restricted fits of columns 1 and 2.

3.2.3. Results for InI

As is illustrated by Fig. 4, the analysis for InI proceeded in much the same manner as that for PbI. The most naturally abundant isotope (96%) of indium is ^{115}In and the analysis was performed using the B_v and D_v constants determined for the ^{115}InI isotopologue. The spectra of the less abundant isotopologues of InI were not intense enough to allow their inclusion in the analysis. Frequencies are available for $R(J)$ transitions for $J = 2 - 7$ for $v = 0 - 2; J = 3 - 7$ for $v = 6$; $J = 4 - 7$ for $v = 4, 5$ and $v = 7 - 10$; $J = 5 - 7$ for $v = 3$ and $v = 11$ of ^{115}InI. In this case, in place of the mid-IR electronic data that better defined the PbI vibrational level spacings for $v = 0 - 3$, the work of Vempati and Jones in the 1980's provides us with ten $A\,0^+ - X0^+$ and seven $B\,1 - X\,0^+$ InI band origins [15, 16], to which we assign uncertainties of ± 0.05 cm^{-1} one lengthy ($J = 6-194$) $R(J)$ branch for the $(4, 4)$ band of the $A\,0^+ - X\,0^+$ system [15] for whose lines we assign uncertainties of ± 0.01 cm^{-1}. and a similarly lengthy ($J = 69 - 270$) mix of P and R- branch lines for the $(1, 1)$ band of the $A\,0^+ - X\,0^+$ for whose lines we assign uncertainties of ± 0.02 cm^{-1}. These results provide us with medium resolution information about vibrational energies for $v'' = 0 - 5$. Moreover, as was the case for PbI, we also have older (in this case, much older) low resolution (± 2 cm^{-1}) band head data from Wehrli and E. Miescher [18] that provides information about the vibrational energies of levels in the extended range $v'' = 0 - 16$. As in Table 2, Table 3 shows the parameter values defining the PEFs for InI obtained, in turn; (i) from our new microwave data alone (column 1); (ii) from a combination of those results with the medium-resolution electronic data spanning $v'' = 0 - 5$ (column 2); (iii) from all of the former plus the 1934 band head data of Wehrli and E. Miescher [18] (column 3). In contrast with the situation for PbI, in this case there is no need to increase the number of PEF 'shape' parameters as we go from one case to the next.

By analogy with Fig. 3, Fig. 5 presents plots of the absolute (*Lower Panel*) and percentage errors (*Upper Panel*) in the vibrational energies generated from the PEFs associated with: the first case considered in Table 3 (MW data only; blue triangular points, curve, and error bars), and from the second case considered in Table 3 (MW and Vempati-Jones data; red square points, curve, and error bars). As for PbI, we find that the errors in the vibrational energies yielded by the PEF

determined from the MW data alone is always less than 1% across the whole domain for which such comparisons are possible. As a final feature of our InI analysis, it seems appropriate to compare the D_v values of Table 2, that were obtained from the original PGOPHER analysis, with values calculated from the potential energy function of the last column of Table 3. Such a comparison is presented in Fig. 6. If the PGOPHER parameter uncertainties are based on 95% rather than 68% confidence limits, they approximately overlap the values generated from our DPF analysis only at low values of v where extensive MW data are available, so perhaps the lesson is that parameters obtained from certain types of PGOPHER analyses should not be trusted too literally. Perhaps a more constructive lesson is that if the PGOPHER fits were repeated with the D_v values fixed at values obtained from the mechanically correct DPF analysis, one would obtain slightly more accurate values of the various v-dependent magnetic splitting parameters.

4. Discussion and Conclusions

It is interesting to reflect on how aspects of broadband rotational spectroscopy (as reported in the opening paragraph of the Introduction) have assisted the analysis performed during this work, and may assist future analyses of potential energy functions on the basis of microwave data. The ability to simultaneously record many transition frequencies is an important advantage given that the analysis that yielded the results of Table 1 involved the measurement of 819 individual transitions. Transition intensities in broadband rotational spectra reflect intrinsic properties of the molecules and gas sample. The rotational spectra of different vibrational states of a given molecule contain very similar splittings and intensity patterns. As a consequence of these factors, the spectra of different v states can be readily distinguished in broadband spectra and rotational transitions can be assigned with quantum numbers with relative ease. Finally, the ability to simultaneously monitor transitions in many different vibrational states presents a useful technical opportunity. Where laser vaporisation is used in combination with supersonic expansion, it is not always easy to rapidly identify the combination of experimental variables (duration of gas pulse, duration of laser pulse, laser power etc) that will yield optimal spectral intensities for a species of interest. It is comparatively straightforward to compare the relative intensities of spectra in different vibrational states by broadband rotational spectroscopy, so allowing optimal experimental conditions to be more easily established.

At this time it is important to recall that the very first report of a DPF analysis of purely rotational data was the analysis of three rotational lines for five isotopologues of Ne-Ar by Grabow *et al.* [29] in 1995. Since that time Grabow and co-workers have performed a number of analyses analogous to those reported here (though without analogs of our Figs. 3 and 5) for SnSe, SnTe,

SiSe, SiTe, PbSe, PbTe, GeSe and GeTe [20–23]. Thus, it is becoming increasingly clear that DPF analysis of v-dependent pure rotational data is a sound and valuable method of determining realistic empirical diatomic molecule potential energy functions, even when no other information is available.

5. Acknowledgements

JHY and RJL are pleased to acknowledge helpful discussions with N. S. Dattani and financial support from NSERC Canada by means of a 'Discovery Grant' awarded to RJL. NRW thanks the European Research Council for a postdoctoral fellowship awarded to SLS, a studentship awarded to JCM and for project funding (No. CPFTMW-307000).

6. Appendix A. Supplementary Data

Supplementary data for this article are available on ScienceDirect (www.sciencedirect.com) and as part of the Ohio State University Molecular Spectroscopy Archives (http://library.osu.edu/sites/msa/jmsa_hp.htm). Supplementary data associated with this article can be found, in the online version, at xxxxxxxxxxxxx. The supplementary data include fits of measured transition frequencies to spectroscopic parameters for each of $v = 0 - 11$. The input files used to perform the potential energy function fits as described in Section 3.2 are also provided.

[1] D. P. Zaleski, S. L. Stephens, and N. R. Walker, Phys. Chem. Chem. Phys. **16**, 25221 (2014).

[2] G. B. Park and R. W. Field, J. Chem. Phys. **144**, 200901 (2016).

[3] C. M. Western, J. Quant. Spectrosc. Radiat. Transfer **00**, 0000 (2016), **PGOPHER**: A program for simulating rotational, vibrational and electronic spectra [http://dx.doi.org/10.1016/j.jqsrt.2016.04.010].

[4] D. P. Zaleski, H. Köckert, S. L. Stephens, N. R. Walker, L.-M. Dickens and C. J. Evans, in 69^{th} International Symposium on Molecular Spectroscopy (University of Illinois, University of Illinois, Champaign-Urbana, Illinois, 2014), paper RE08.

[5] C. J. Evans, L.-M. E. Needham, N. R. Walker, H. Köckert, D. P. Zaleski, and S. L. Stephens, J. Chem. Phys. **143**, 244309 (2015).

[6] K. Ziebarth, R. Breidohr, O. Shestakov, and E. H. Fink, Chem. Phys. Lett. **190**, 271 (1992), .

[7] B. Popov and H. Neujmin, Phys. Z. Sowjetunion **2**, 394 (1932).

[8] G. D. Rochester, Proc. Roy. Soc. (London) **153**, 407 (1936).

[9] G. D. Rochester, Proc. Roy. Soc. (London) **167**, 567 (1938).

[10] K. Wieland and R. Newburgh, Helv. Phys. Acta. **25**, 87 (1952.

[11] G. Rodriguez, C. M. Herring, R. D. Fraser, and J. G. Eden, J. Opt. Soc. Am. B **13**, 1362 (1996).

[12] A. H. Barrett and M. Mandel, Phys. Rev. **109**, 1952 (1958).

[13] B. Schenk, E. Tiemann, and J. Hoeft, Z. Naturforsch. A. **25**, 1827 (1970).

[14] N. R. Walker, S. G. Francis, J. J. Rowlands, and A. C. Legon, J. Mol. Spectrosc. **239**, 126 (2006).

[15] S. N. Vempati and W. E. Jones, J. Mol. Spectrosc. **120**, 441 (1986).

[16] S. N. Vempati and W. E. Jones, J. Mol. Spectrosc. **122**, 190 (1987).

[17] S. N. Vempati and W. E. Jones, J. Mol. Spectrosc. **127**, 232 (1988).

[18] M. Wehrli and E. Miescher, Helv. Phys. Acta. **7**, 298 (1934).

[19] S. L. Stephens, W. Mizukami, D. P. Tew, N. R. Walker, and A. C. Legon, J. Chem. Phys. **136**, 064306 (2012).

[20] L. Bizzocchi, B. M. Giuliano, M. Hesse, and J.-U. Grabow, J. Chem. Phys. **126**, 114305 (2007).

[21] B. M. Giuliano, L. Bizzocchi, and J.-U. Grabow, J. Mol. Spectrosc. **251**, 261 (2008).

[22] B. M. Giuliano, L. Bizzocchi, S. Cooke, D. Banser, M. Hesse, J. Fritzsch, and J.-U. Grabow, Phys. Chem. Chem. Phys. **10**, 2078 (2008).

[23] B. M. Giuliano, L. Bizzocchi, R. Sanchez, P. Villanueva, V. Cortijo, M. E. Sanz, and J.-U. Grabow, J. Chem. Phys. **135**, 084303 (2011).

[24] R. J. Le Roy, J. Quant. Spectrosc. Radiat. Transfer **000**, 0000 (2016), **dPotFit :** A Computer Program to Fit Diatomic Molecule Spectral Data to Potential Energy Functions: [http://dx.doi.org/10.1016/j.jqsrt.2016.06.002].

[25] E. G. Lee, J. Y. Seto, T. Hirao, P. F. Bernath, and R. J. Le Roy, J. Mol. Spectrosc. **194**, 197 (1999).

[26] J. Y. Seto, Z. Morbi, F. Charron, S. K. Lee, P. F. Bernath, and R. J. Le Roy, J. Chem. Phys. **110**, 11756 (1999).

[27] R. J. Le Roy, D. R. T. Appadoo, K. Anderson, A. Shayesteh, I. E. Gordon, and P. F. Bernath, J. Chem. Phys. **123**, 204304 (2005).

[28] R. J. Le Roy and A. Pashov, J. Quant. Spectrosc. Radiat. Transfer **00**, 0000 (2016), **betaFIT :** A Computer Program to Fit Pointwise Potentials to Selected Analytic Functions: [http://dx.doi.org/10.1016/j.jqsrt.2016.03.036].

[29] J.-U. Grabow, A. Pine, G. Fraser, F. Lovas, R. Suenram, T. Emilsson, A. Arunan, and H. S. Gutowsky, J. Chem. Phys. **102**, 1181 (1995).

Table 1 Fitted constants associated with ground and vibrational excited states of ^{115}InI.[1] Numbers in parentheses are the 95% confidence limit uncertainties in the last digits shown for each parameter.

	ν=**0**	ν=**1**	ν=**2**	ν=**3**
B_v/MHz	1103.68715(50)	1100.57132(46)	1097.45956(60)	1094.35366(98)
D_v/Hz	188.9(52)	192.4(44)	184.4(60)	187.0(94)
C^{I}/kHz	4.81(46)	4.26(72)	4.3(11)	4.9(17)
C^{In}/kHz	5.36(40)	4.43(44)	4.70(62)	5.9(11)
χ^{I}/MHz	−387.890(42)	−389.71(11)	−391.75(14)	−393.17(24)
χ^{In}/MHz	−607.320(48)	−605.388(90)	−603.29(13)	−601.03(40)
N	96	163	122	79
σ/kHz	10.2	10.3	11.8	14.1
	ν=**4**	ν=**5**	ν=**6**	ν=**7**
B_v/MHz	1091.25241(90)	1088.15849(82)	1085.0668(12)	1081.9793(12)
D_v/Hz	185.1(94)	203.7(84)	202(14)	178(14)
C^{I}/kHz	4.2(22)	[4.81][1]	[4.81]	[4.81]
C^{In}/kHz	4.7(12)	[5.36][1]	[5.36]	[5.36]
χ^{I}/MHz	−395.22(40)	−397.50(38)	−399.10(36)	−401.60(80)
χ^{In}/MHz	−599.94(42)	−597.24(36)	−595.38(36)	−593.31(64)
N	62	68	45	45
σ/kHz	11.7	12.7	11.7	13.8
	ν=**8**	ν=**9**	ν=**10**	ν=**11**
B_v/MHz	1078.89877(96)	1075.8248(13)	1072.7503(18)	1069.6902(22)
D_v/Hz	184.9(96)	207(14)	162(17)	228(26)
C^{I}/kHz	[4.81]	[4.81]	[4.81]	[4.81]
C^{In}/kHz	[5.36]	[5.36]	[5.36]	[5.36]
χ^{I}/MHz	−404.49(46)	−405.58(86)	−406.0(10)	−408.6(12)
χ^{In}/MHz	−590.60(30)	−588.77(84)	−587.2(12)	−584.4(13)
N	53	38	22	26
σ/kHz	11.9	13.8	10.9	12.8

[1] Values in square brackets are fixed to the results for the $v = 0$ state.

Table 2 Parameters defining the recommended EMO potential energy and BOB correction functions for the $X\,^2\Pi_{1/2}$ state of PbI obtained from a fit to the $v'' = 0 - 5$ MW data alone [5] (column 1), from those MW data plus the $X2 - X1$ band heads of Ziebarth *et al.* [6] (column 2), and from the full data set including UV band heads of Rodriguez *et al.* [11] (column 3). Numbers in parentheses are the 95% confidence limit uncertainties in the last digits shown for each parameter. Square brackets are placed around a parameter value held fixed in the fit. All fits were performed with $q = 3$ and with fixed $\mathfrak{D}_e = 20500$ cm^{-1}.

	MW data alone	MW & near IR data	MW & IR &UV data
r_e/Å	2.797 603 9 (3)	2.797 603 73 (50)	2.797 604 6(17)
β_0	1.22035 (440)	1.21494 (14)	1.21477 (88)
β_1	−0.0142(14)	−0.01587 (15)	−0.01522 (75)
β_2	0.241 (6)	0.234 (14)	0.24 (15)
β_3	–	–	−0.19 (14)
β_4	–	–	4.2 (18)
$u_1^{\rm Pb}$/cm^{-1}	7.0 (19)	7.0 (58)	[7.0]
$\overline{dd}(MW)$	0.132	0.138	0.296
$\overline{dd}(IR)$	–	1.014	1.041
$\overline{dd}(UV)$	–	–	1.539

Table 3 Parameters defining the recommended EMO potential energy functions of the $X\,^1\Sigma$ state of InI obtained from a fit to the $v'' = 0 - 11$ MW data alone [5] (column 1), from those MW data plus the medium resolution Vempati and Jones [15, 16] $A\,0^+ - X\,0^+$ and $B\,1^+ - X\,0^+$ data for $v'' = 0 - 5$ (column 2), and from the full data set including the low resolution $A\,0^+ - A\,0^+$ band heads of Wehrli and Miescher [18] (last column). Numbers in parentheses are the 95% confidence limit uncertainties in the last digits shown for each parameter. All fits were performed with $q = 3$ and with fixed $\mathfrak{D}_e = 25654.8$ cm^{-1}.

	MW data alone	MW + Vempati-Jones data	all data
r_e	2.753 650 6 (5)	2.753 649 44 (6)	2.753 649 7(5)
β_0	1.05086 (670)	1.044 153 (340)	1.044 387 (460)
β_1	−0.13257 (55)	−0.133 114 (36)	−0.133 094 (70)
β_2	−0.006 (30)	0.1287 (370)	0.0902 (560)
β_3	0.19 (4)	−0.031 (63)	0.03 (9)
β_4	–4	0.21 (9)	0.15 (10)
$\overline{dd}(MW)$	0.747	0.763	0.764
$\overline{dd}$(Vempati-Jones)	–	0.835	0.835
$\overline{dd}$(Wehrli)	–	–	0.585

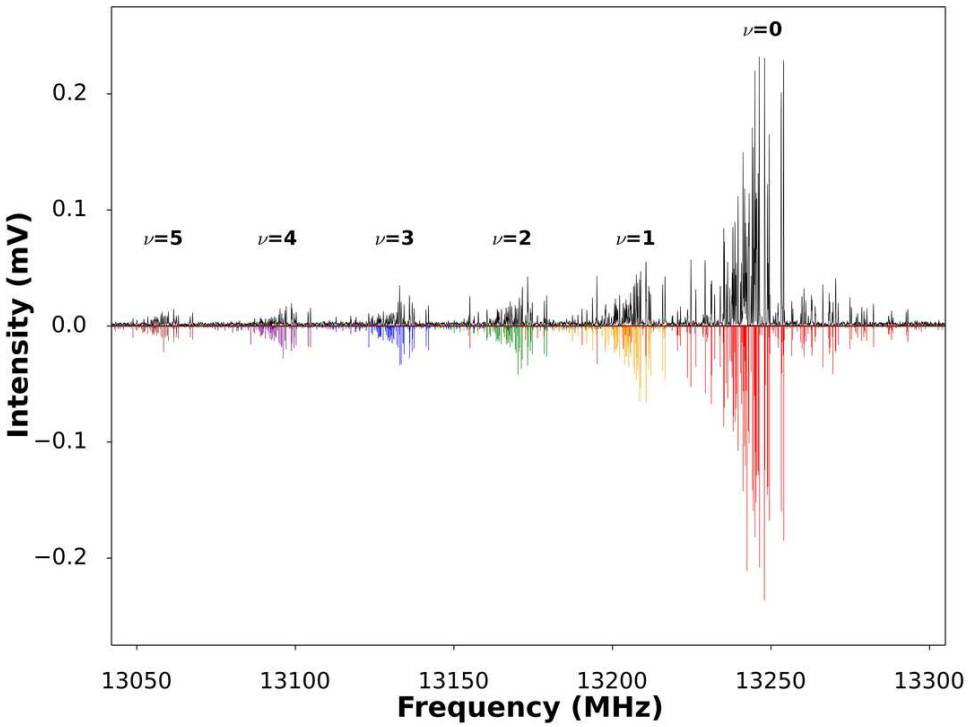

Figure 1. A section of the rotational spectrum recorded for InI displaying transitions in a series of vibrational states. The experimentally-measured spectrum is displayed in black. Simulated $J' \rightarrow J'' = 7 \rightarrow 6$ transitions in v=0 (red), v=1 (orange), v=2 (green), v=3 (blue), v=4 (purple) and v=5 (grey) states are constructed from fitted values of spectroscopic parameters (see Table 1) and are displayed inverted. 44k FIDs were averaged to record the displayed spectrum (data collected over about 3 hours of real time).

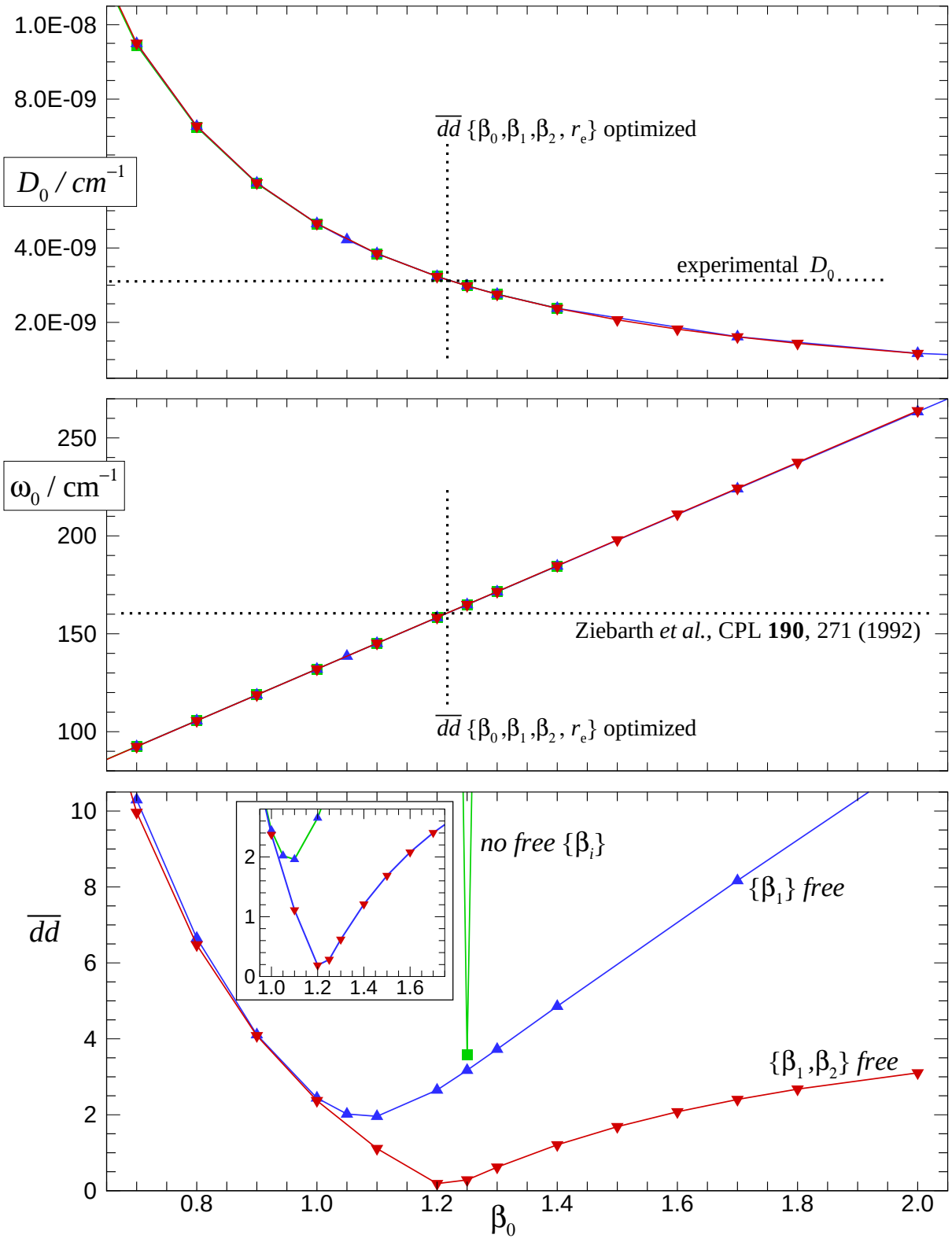

Figure 2. Overview of results of the fits for PbI. *Bottom Panel*: quality-of-fit parameter $\overline{dd}$ plotted *vs.* a fixed value of β_0 for fits in which r_e and other β_i parameters fitted freely. *Middle panel*: fundamental vibrational level spacing $\omega_0 \equiv G(v=1) - G(0)$ of the PEFs determined from these fits, with the value determined from the electronic $X2 - X1$ study of Ziebarth *et al.* [6] shown as a dotted horizontal line. *Top Panel*: value of the leading centrifugal distortion constant $D_{v=0}$ calculated from the PEFs yielded by the various fits, with the experimental value from Ref. [5] shown as a horizontal dotted line.

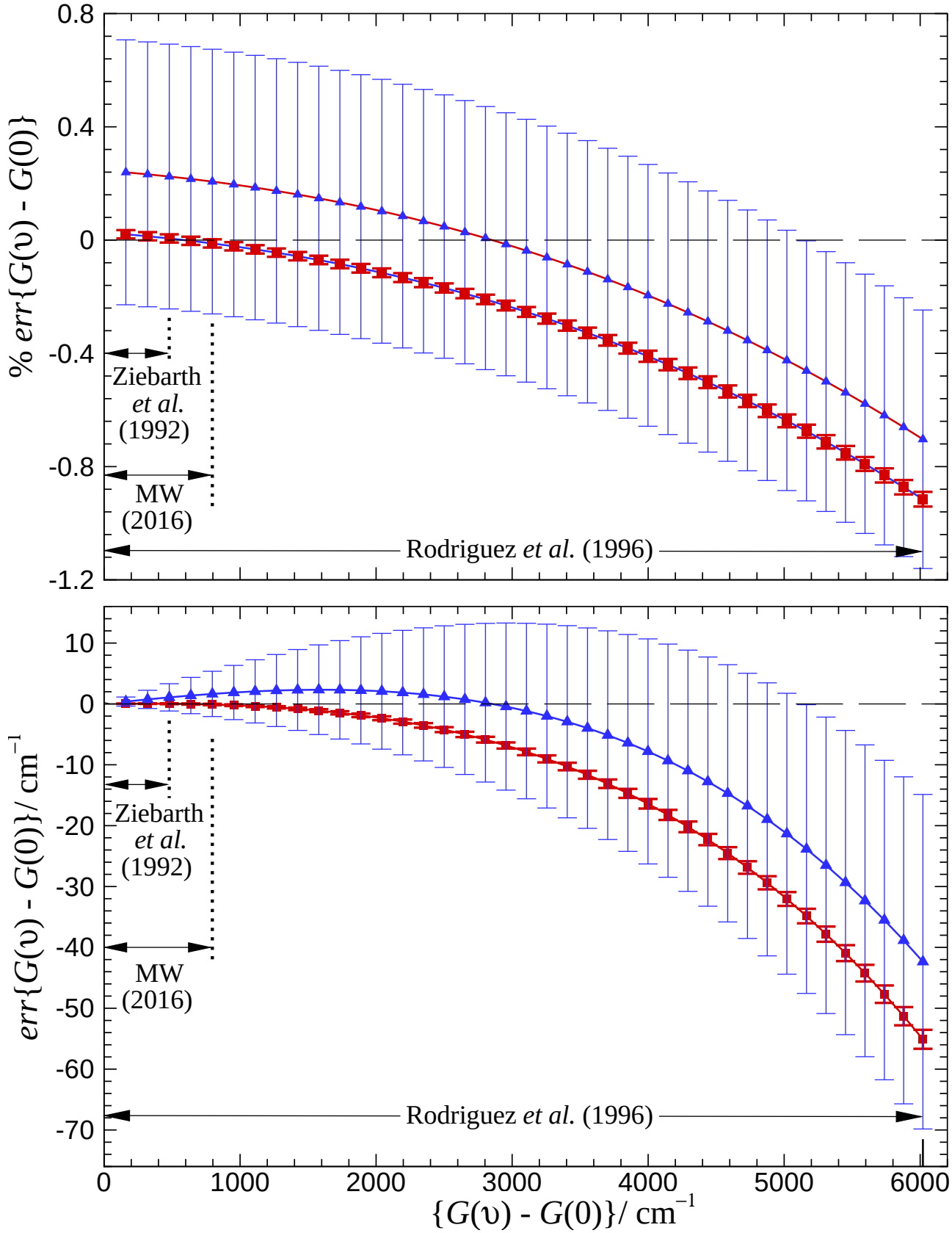

Figure 3 *Lower Panel*: discrepancies from the optimal estimates of the vibrational overtone energies $\{G(v) - G(0)\}$ yielded by the PEF for PbI determined from the full ($v = 0 - 40$) data set, (i) of vibrational energies from the PEF determined from only the MW data for $v = 0-5$ (blue triangular points, uncertainty bars, and curve), and (ii) of vibrational energies from the PEF determined from those MW data and from the IR (electronic band heads spanning $v'' = 0 - 4$, red square points, uncertainty bars and curve). *Upper Panel*: those discrepancies and their uncertainties as a percentage of the associated overtone energies.

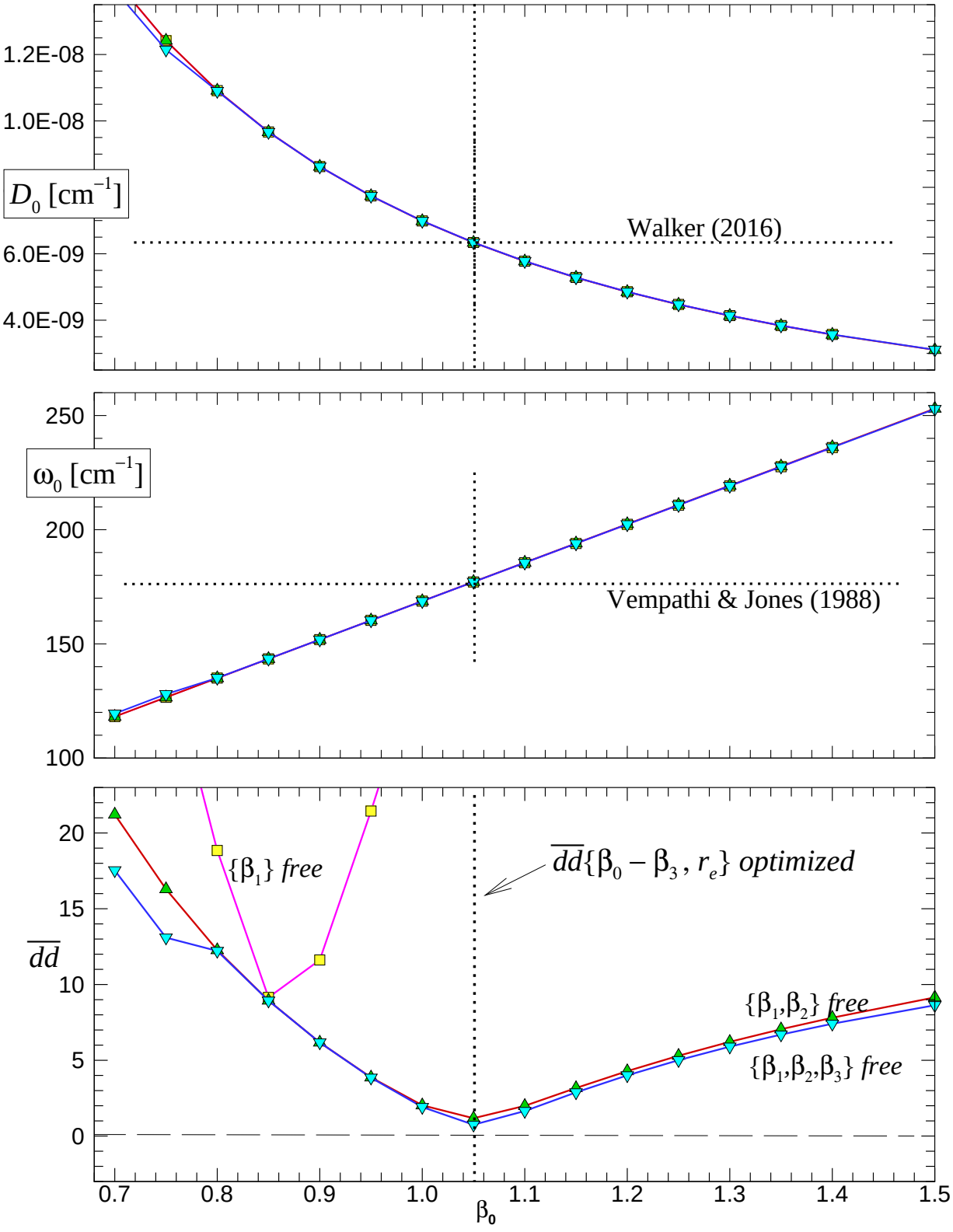

Figure 4. Overview of results of the fits for InI: as in Fig. 2.

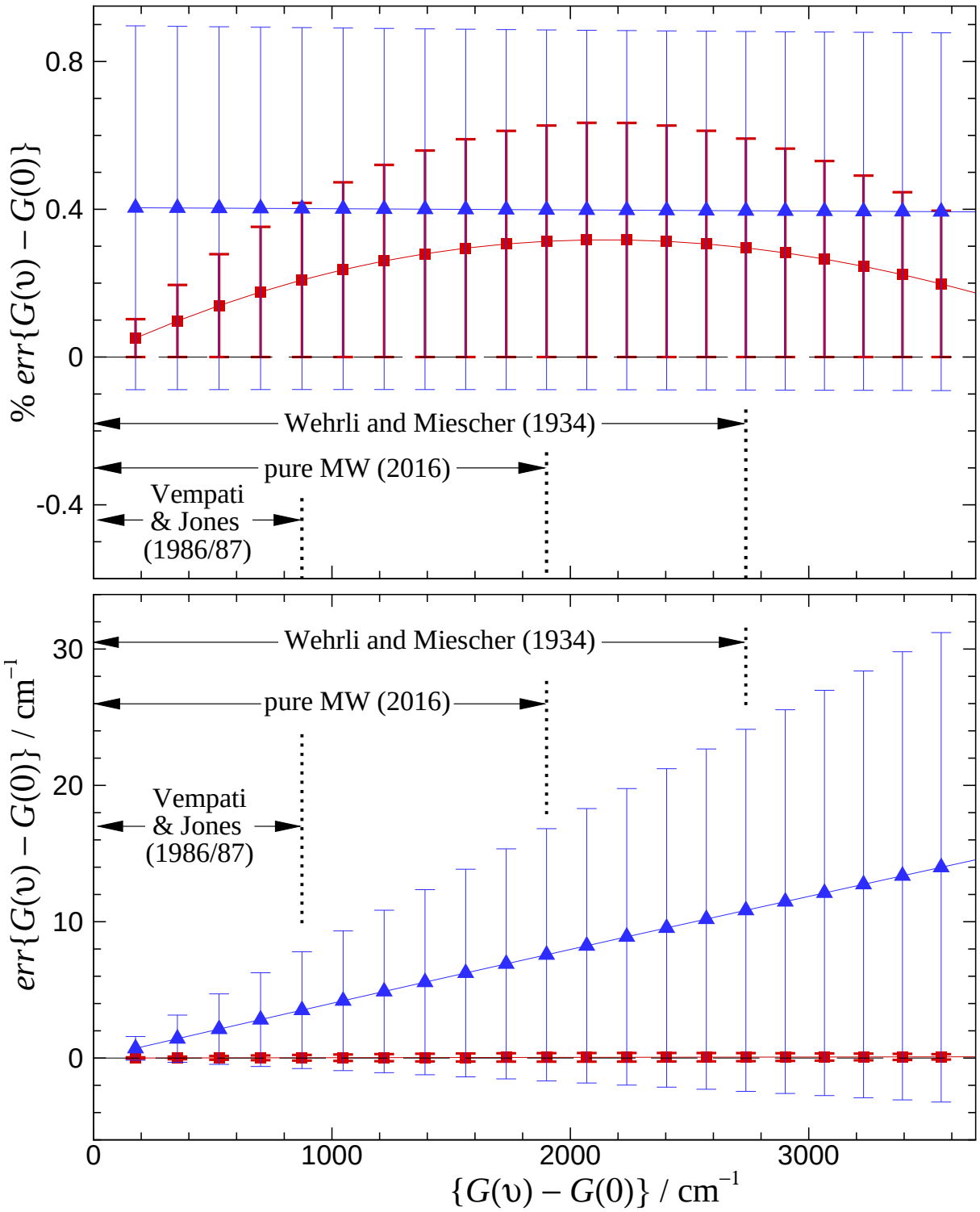

Figure 5. Absolute (*Lower Panel*) and percentage (*Upper Panel*) errors in vibrational energies generated from the PEF for InI determined from our MW data alone (blue triangular points, uncertainties and curves) and that determined from the combination of the MW data with the low-v' electronic data of Vempati and Jones [15, 16] (red square points, uncertainties and curves).

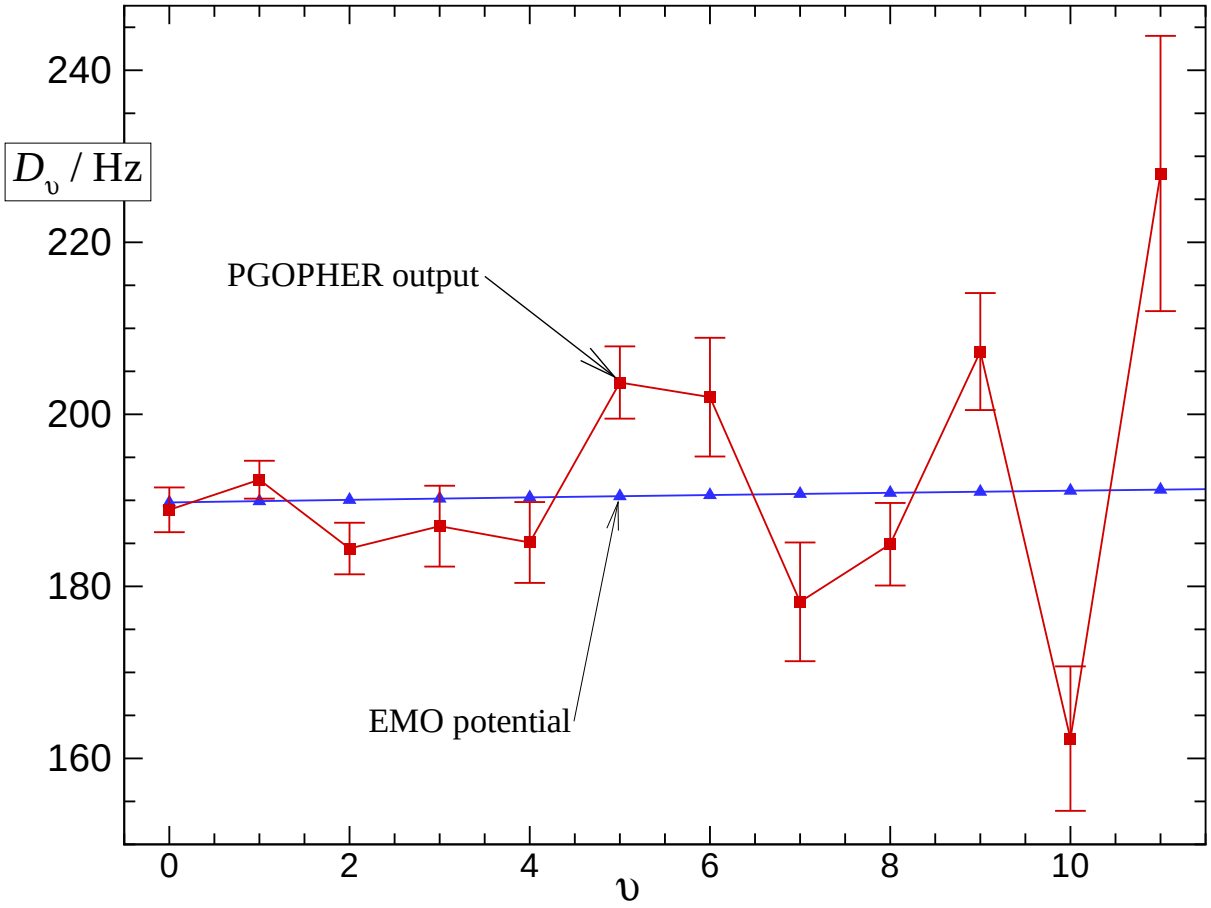

Figure 6. Comparison of D_v values obtained from the initial PGOPHER analysis (red square points, error bars, and lines), with those generated from the EMO potential of the last column of Table 3. The error bars shown are 95% confidence limit uncertainties on the results of the PGOPHER analysis.